

## Major-element analysis of cyclic black shales: Paleooceanographic implications for the Early Cretaceous deep western Tethys

Ulrich G. Wortmann

Geological Institute, Eidgenössische Technische Hochschule Zürich, Switzerland

Reinhard Hesse

Departement of Earth and Planetary Sciences, McGill University, Montréal, Québec, Canada

Wolfgang Zacher

Lehrstuhl für Allgemeine, Angewandte und Ingenieur Geologie der Technischen Universität München, Germany

**Abstract.** Lower Cretaceous sediments are frequently characterized by a well expressed cyclicity. While the processes influencing environments above the carbonate compensation depth (CCD) are reasonably well understood, almost nothing is known about the deep ocean. Cretaceous sub-CCD sediments from the Tethys and Atlantic Oceans typically show rhythmic black/green shale successions. To gain insight into the nature of these black/green shale cycles, we performed detailed geochemical analyses (X-ray fluorescence, Rock-Eval and reactive iron analysis) on a 3 m long section of latest Aptian age. The major-element distribution of the analyzed shale sequence indicates a periodic change from a high-productivity and well-oxygenated green shale mode to a low-productivity oxygen-deficient black shale mode. It is proposed here that the preservation of organic matter was dependent on the strength of salinity-driven deepwater generation. Furthermore, the data show that the  $C_{Org}$  content covaries with changes in the detrital composition. Therefore we hypothesize that Tethyan deepwater circulation was sensitive to changes in the monsoonal system. Time series analysis suggests that these changes are periodic in nature, although we are currently unable to prove that the dominant periodicity is related to the precession component of the Milankovitch frequencies.

### 1. Introduction

Starting with the seminal paper of *Ryan and Cita* [1977], geologists in the late 1970s began to recognize the widespread distribution and economic significance of Cretaceous black shales, which were discovered in all major ocean basins spanning most marine depositional environments. In order to explain these black shale occurrences, different models have been proposed. *Schlanger and Jenkyns* [1976] suggested ocean-wide anoxia. *Degens and Stoffers* [1976] used the East

African rift lakes as an analogy. *Weissert et al.* [1978] and *Arthur and Premoli Silva* [1982] concluded that the cyclic black shales of the Southern Alps and central Italy were caused by periodic overturn in deep anoxic basins. *Dean et al.* [1978], *Jansa et al.* [1979] and *Dean and Gardner* [1982] argued that cyclic black shale sedimentation was caused by turbidity currents, whereas *Habib* [1982] attributed black shale layers to times of massive input of terrestrial organic matter. Later studies challenged the role of anoxia in black shale formation because it became apparent that anaerobic decomposition of organic matter (OM) can be as fast as aerobic decomposition [*Kristensen and Blackburn*, 1987; *Canfield*, 1989b]. Furthermore, it appeared that the distribution of Quaternary organic-rich facies may be unrelated to the presence of anoxic bottom water conditions but is instead controlled by the amount of primary production [*Pedersen and Calvert*, 1990]. Newer studies emphasize that the deposition of black shales depends on many factors, like primary production, oxygenation level of the water column, overall sedimentation rate, distance from the coast, and water depth, all of them influencing burial rate of OM [*Berner*, 1978; *Canfield*, 1989b; *Calvert and Pedersen*, 1992; *Canfield*, 1994; *Keil et al.*, 1994; *Calvert et al.*, 1996].

Most of the described Early Cretaceous black shales accumulated in the Atlantic and Tethys Oceans, which at that time was a small appendix to the world ocean (Figure 1). The Tethyan Early Cretaceous sediments are generally characterized by a well expressed cyclicity. Depending on the depositional environment, these cycles are either expressed as carbonate/marl, marl/shale or black/green shale alternations. *De Boer* [1982], *de Boer and Wonders* [1984] and *Fischer et al.* [1991] showed that the pelagic carbonate/marl rhythms correspond to the precession component, while *Park and Herbert* [1987] were able to demonstrate that marl/black marl cycles correspond to the obliquity and eccentricity com-

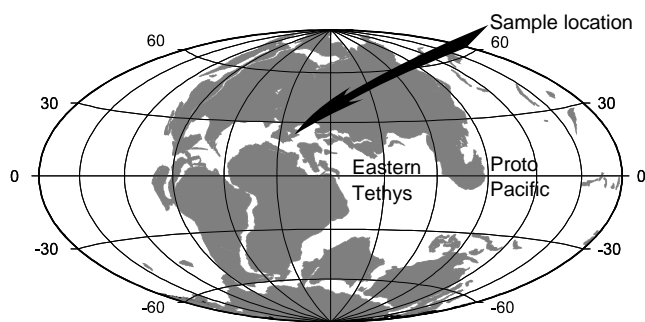


**Figure 1.** Ocean basin boundaries of the Early Aptian using the 2000 m isobath. When viewed using an equal area projection (Hammer), it becomes readily apparent that the Atlantic and Tethys Oceans are only a small appendix to the proto Pacific, covering only one twelfth of the global ocean area. Even if we include the eastern Tethys between Australia and Asia, the ratio is still less than one sixth. The map was generated by the Ocean Drilling Stratigraphic Network Plate Tectonic Reconstruction Service (<http://www.odsn.de/odsn/services/paleomap/paleomap.html>) using the data of Hay *et al.* [1999b].

ponents of the Milankovitch frequencies. It has been suggested that the black/green shale couples probably spanned periods from 20 to 50 kyr in the Milankovitch range of periodicities [e.g., Dean *et al.*, 1978; Arthur and Premoli Silva, 1982], but it has never been possible to relate directly the occurrence of rhythmic black/green shales to Milankovitch cycles. Therefore, the objectives of this study were threefold: (1) to determine the nature and possible cause of the cyclic black/green color changes by means of geochemical analysis, (2) to test by means of frequency analysis whether these rhythms are related to Milankovitch forcing or not, and (3) To derive a reasonable explanation for the interaction between external forcing factors and deep-sea sedimentation below the calcite compensation depth (CCD).

### 1.1. Geologic Setting

While the record of cyclic sedimentation above the CCD has gained wide attraction, almost nothing is known about the deep Cretaceous Tethys and Atlantic. Unfortunately, the Ocean Drilling Program/Deep Sea Drilling Project (ODP/DSDP) data and cores from the sub-CCD parts of the Cretaceous Atlantic Ocean are sparse. Similarly, almost all preserved Tethyan sediments have been deposited on continental crust and thus yield no record of the deep ocean. We therefore searched for a location that has a complete sub-CCD record from the Aptian/Albian, is reasonably well defined in terms of biostratigraphy, and is well enough preserved to allow for geochemical investigations. To our knowledge, only a few such locations exist. One of them is the Rhenodanubian Supergroup, north of the Northern Calcareous Alps

in South Germany (Fig. 2).

This Early Cretaceous to early Eocene supergroup consists of turbidite-dominated formations, recording more than 70 m.y. of deep-sea sedimentation [Hesse, 1974, 1982]. The middle Barremian to Albian Rehbrein-graben Formation (also known as “Flysch-Gault”), constitutes a 200 m thick succession. The middle Barremian to the base of the Aptian and the complete Albian are dominated by pelagic clays, while the Aptian shows a characteristic tripartitioning: a sandstone member in the Early Aptian, pelagic shales in the Middle Aptian, and a second sandstone member in the Late Aptian. The pelagic shales of the entire section are characterized by a striking black/green shale rhythmicity, the individual color intervals ranging from 5 to 50 cm in thickness. The sedimentology, visual appearance, and geochemistry are similar to shale sequences in cores from the Cape Verde basin along the continental margin of northwest Africa [see, e.g., Dean *et al.*, 1978; Brumsack, 1980].

As a result of the paleodepth below the CCD Hesse [1975] and the corresponding paucity of fossils, dating is a problem. The base of the Rehbrein-graben Formation was dated by means of paleomagnetostratigraphy as middle Barremian (top of magnetochron M3) [Hauck, 1998], while the sampled interval could be dated as latest Aptian on the basis of  $\delta^{13}\text{C}_{\text{Org}}$  isotope stratigraphy (to be published elsewhere). The upper boundary of the Rehbrein-graben Formation (225 m above the middle Barremian) is dated by the occurrence of *Calculites anfractus* as terminal Albian/Early Cenomanian age (CC9a of) [Sissingh, 1978]. Using the timescale of Gradstein *et al.* [1995], we estimate 225 m of accumulation within 24 m.y., resulting in an average sedimentation rate of  $9.4 \text{ mm kyr}^{-1}$ . Since the amount of sediment eroded by turbidity currents is unknown, this is a minimum estimate.

The paleogeographic position of the Rhenodanubian Supergroup is still a matter of debate, but paleomagnetic, geologic, and faunal evidence [Hauck, 1998; Wortmann, 1996] suggests a position east of Spain and west of the Apulian plate [Wortmann, 1996]. The paleoenvironment was described by Hesse [1974] and Hesse and Butt [1976] as a trench abyssal plain below the CCD. The paleotectonic setting can be best described in terms of a transform system [Hsü, 1972; Hesse, 1982; Wortmann, 1996]. The paleoposition of this section was either close to or within the oceanic gateway between the Atlantic and Tethys Ocean, which makes it an ideal site to investigate questions of Cretaceous deepwater circulation and paleoclimate.

### 1.2. Methods

For geochemical analysis we took 104 samples from a 3 m outcrop interval in Breitenbach Creek near “Bad Wiessee” (Figure 2). This site contains only the late Aptian to early Albian record but was preferred over the

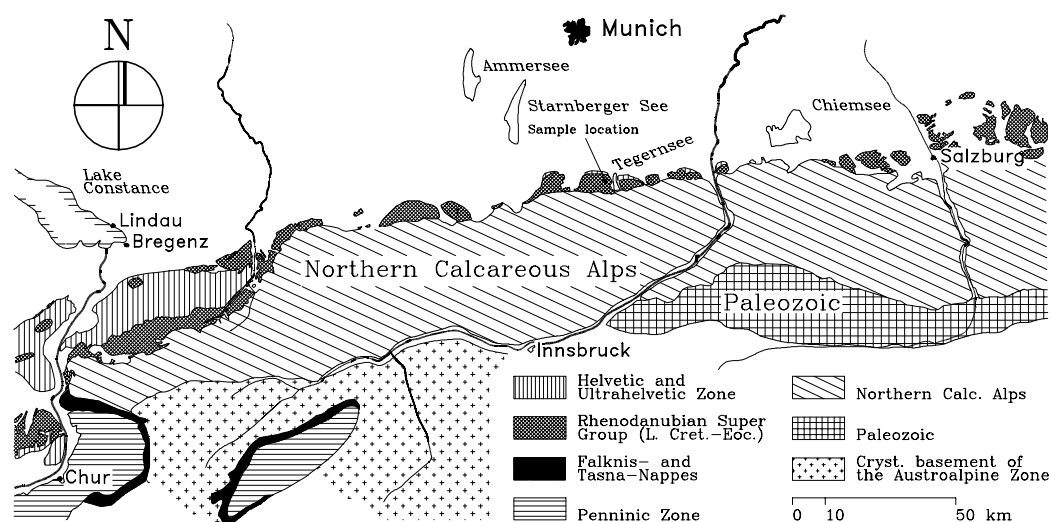


**Figure 2.** Simplified geological map showing the outcrop area of the Rhenodanubian Supergroup in the Bavarian part of the East Alps (South Germany; modified after *Vetters* [1923]). The sample location of the Breitenbach Creek near Bad Wiessee is indicated by the arrow below the Starnberger See. Details concerning how to access the section are given by *Wortmann* [1996].

type section (Rehbrein Creek) because of better outcrop conditions. Applying the estimated sedimentation rate of  $9.4 \text{ mm kyr}^{-1}$ , the sampled section covered  $\sim 320$  kyr with a resolution of 1.1–4.3 kyr per sample, depending on sample thickness (1–4 cm). The implicit assumption of a linear accumulation rate is backed by the observation that the mean thickness of the black shales (measured over the whole Aptian Albian section) is similar to the mean thickness of the green shales.

The strategy in selecting analytical methods was that they should be sufficiently fast and cost effective to allow for continuous high-resolution sampling and provide information about biogenic processes in the water column, detrital input, and the redox state of the water and the sediment. We thus selected a suite of primarily major elements that can easily be determined by X-ray fluorescence analysis (XRF) and have been successfully used to deduce changes in biogenic productivity and detrital input previously [e.g., *Calvert et al.*, 1996].

Total sulfur (TS) and total carbon (TC) were determined by means of a Leco device. Total organic carbon (TOC) was determined by Leco measurements of decarbonated samples (12 hours with 12 N HCl). The inorganic carbon (IC) content was calculated as

$$\text{IC}(\text{wt } \%) = \text{TC}(\text{wt } \%) - \text{TOC}(\text{wt } \%)$$

Carbonate content was calculated as  $\text{CaCO}_3 = \text{IC} \times 8.333$ . Reactive iron ( $\text{Fe}_x$ ) is used here in the sense of *Leventhal and Taylor* [1990] who define  $\text{Fe}_x$  to comprise non-silicate-bound iron, amorphous iron oxides or oxyhydroxides, FeS and also some crystalline iron oxides. As per standard conventions,

we assume that  $\text{Fe}_x$  equals the HCl-extractable iron content of the sediment [*Berner*, 1970; *Raiswell et al.*, 1988; *Leventhal and Taylor*, 1990]. Thus  $\text{Fe}_x$  was determined by leaching the samples in 1 N HCl for 12 hours and analyzing the leachate using atomic absorption spectrometry (AAS). Pyrite-bound iron was calculated from TS as  $\text{Fe}_{\text{Py}} = \text{TS} \times 0.871$  assuming that all sulfur is bound to pyrite. The “degree of pyritization” (DOP) [*Raiswell et al.*, 1988] was calculated as

$$\text{DOP} = \frac{\text{Fe}_{\text{Py}}}{\text{Fe}_{\text{Py}} + \text{Fe}_x}$$

Optical assessment of the OM was performed on polished sections as well as on OM concentrates. The OM concentrates were first decarbonated with HCl (30%). In a second step, minerals were removed using HF (40%). Finely dispersed OM was then removed with a  $14 \mu\text{m}$  sieve. For chemical assessment of the OM we used Rock-Eval pyrolysis [*Espitalié et al.*, 1985a, b]. This technique yields four parameters: S1, hydrocarbons (HC) already present in the rock that are volatilized by heating to  $200^\circ\text{C}$ ; S2, HC and related compounds generated at higher temperatures by pyrolysis of insoluble kerogen; S3, carbon dioxide and water; and  $T_{\text{max}}$ , the pyrolysis temperature at which the maximum release of HC has occurred. From these numbers the hydrogen index (HI), which can be used to classify the source of the OM, is calculated as  $\text{HI} = \text{S2}/\text{TOC}$ . The production index, which is used to characterize the maturity of the OM, is calculated as  $\text{S1}/(\text{S1} + \text{S2})$ .

Quartz content and clay mineralogical composition were analyzed by X-ray powder diffraction. Kaolinite

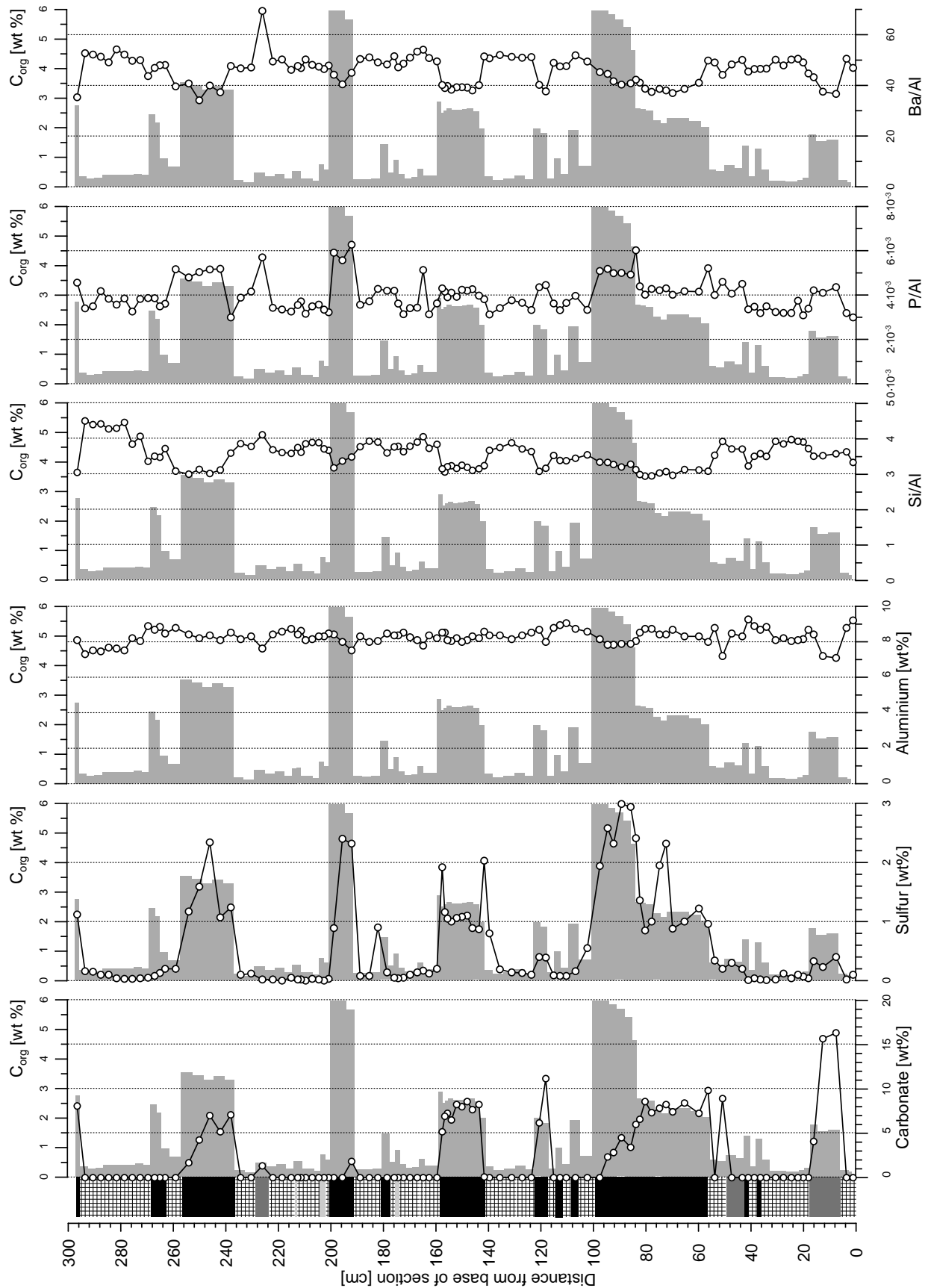


**Figure 3.** Measured concentrations of carbonate, S, Al (wt %), and Si/Al, P/Al, and Ba/Al (wt %/wt %) plotted against total organic carbon (wt %) and lithology. (left) shale colors as observed in field: black and shaded areas indicate black or grey shales, respectively, the crosshatched pattern indicates green shales. Each curve is superposed

was differentiated from chlorite by means of dimethyl sulfoxide (DMSO) treatment following procedures by Calvert [1984]. All results refer to the bulk composition of the sample and are expressed in weight percent or as elemental weight ratios. Assuming that aluminium is of detrital origin, all results are normalized to Al to compensate for changes in the ratio of the biogenic versus detrital flux [see, e.g., Calvert and Pedersen, 1993]. Recent work showed that Al can also be influenced by the biogenic flux [Murray et al., 1993]. However, this work was done in an equatorial upwelling area with high primary production rates. Unlike the data presented by Murray et al. [1993], our data show no correlation between the Al and organic carbon ( $C_{Org}$ ) content of the sediment. Even more important, the Al distribution shows only a minor overall variation, and does not covary with the Ti and Zr nor with the Ba and Si data (Figure 3).

The possible influence of weathering was determined by sampling an individual black shale layer from the fresh rock into the weathering zone of the outcrop and incorporating the results into the error estimates. Though all collected samples are considered to be unweathered, we used these maximum error estimates since local weathering along microscopic joints could not be excluded. For all data presented the systematic and statistical errors, including error propagation, have been calculated at a significance level of 95% (Table 1). An absence of error bars in the plots indicates that the errors are less than the dimensions of the plot symbol used.

Time series analysis was carried out using the geochemical results from the 104 analyzed samples. Since we were unable to recover samples of identical thickness, we used the Lomb-Scargle transformation, which is designed to handle unevenly spaced data [Scargle, 1992]. Although our graphs show the power distribution beginning with a period length of 2 cm, the reader should keep in mind that with a maximum sample thickness of up to 4 cm, no reliable information can be gained below a period length of 8 cm.

## 2. Results

Compared to the green shales, the black shales show characteristically lower ratios for Si/Al, Ba/Al, Na/Al and K/Al, as well as characteristically greater values for nearly all other elemental ratios (see Figure 3–5, the numerical values are given in Wortmann [1999]). Furthermore, the black shales are laminated while the green shales are affected by bioturbation. Calculation of the DOP of the black shales yields values from 0.63 to 0.91, indicating conversion of nearly all reactive iron to pyrite and deposition under reducing conditions [Raiswell and Berner, 1985, 1986]. From a ternary plot with the poles of  $Fe_x$  plus  $Fe_{Py}$  (i.e., total reactive iron),  $C_{Org}$ , and TS

we can draw important conclusions about pyrite formation [Dean and Arthur, 1989]. If samples plot along a line of constant TS/ $C_{Org}$  ratio, carbon was the limiting factor. If no systematic relation is observable, sulfur limitation is likely. If samples plot along a line of constant TS/total  $Fe_x$  ratio, as in the present study, pyrite formation was iron-limited (Figure 6). Since  $Fe_{Py}$  was calculated under the assumption that  $S_{Py}$  equals TS, TS and total reactive iron are not independent. However, assuming additional sulfur phases would reduce the amount of total reactive iron even more.

Optical assessment of the OM on polished black shale samples shows a fluorescent matrix of marine OM with dark laminations formed by mineral layers. The kerogen concentrates show only minor amounts of kerogen flakes, while structured components and dark inertinite particles dominate. The structured kerogen is dominated by algae, while pollen and spores are sparse. Optical determination of vitrinite reflectance yields values of  $R_r$  between 0.65 and 0.89 ( $\Delta_{95\%} = \pm 0.003$ ), indicating the upper limit of an immature source rock [Tissot and Welte, 1984]. This is in good agreement with the  $T_{max}$  parameter (431–438°C) of the Rock-Eval analysis and the production index (0.09) [Teichmüller and Durand, 1983].

Using S2 to calculate HI yields values up to 140, suggesting terrestrial and/or degraded marine OM [Tyson, 1987]. However, indirect determination of the HI using the method of Langford and Blanc-Valleron [1990] yields a value of 250 (Figure 7). Calculating the matrix effect following Langford and Blanc-Valleron [1990] shows that up to 5.4 mg HC per gram sample mass may have been adsorbed by the rock matrix and have not been detected by S2, explaining the large difference in the measured and calculated HI values.

Examination of smears shows that the carbonate found within the black shales consists mainly of detrital calcite, a small amount of rhomboidal dolomite ( $\leq 10 \mu m$ ) and some coccoliths. The clay mineralogy is dominated by chlorite, kaolinite, illite, illite/smectite, and other mixed layer minerals. Major differences in the clay-mineral composition between the green and the black shales could not be detected. However, the combined chlorite/kaolinite peak is stronger in the black shale samples than in the green shale samples – a relationship that is commonly observed in the Early Cretaceous [e.g., Chamley and Robert, 1982, Figure 2].

### 2.1. Interpretation of the Analytical Results

The most visible differences between the black and the green shales are the content of OM and color. While the greenish color points to reduced iron, the black color may be caused by finely dispersed pyrite [McCave, 1979] or oxidized OM [Habib, 1982]. The bioturbation of the green shales indicates oxygenated bottom water, while the lamination of the black shales proves the absence of

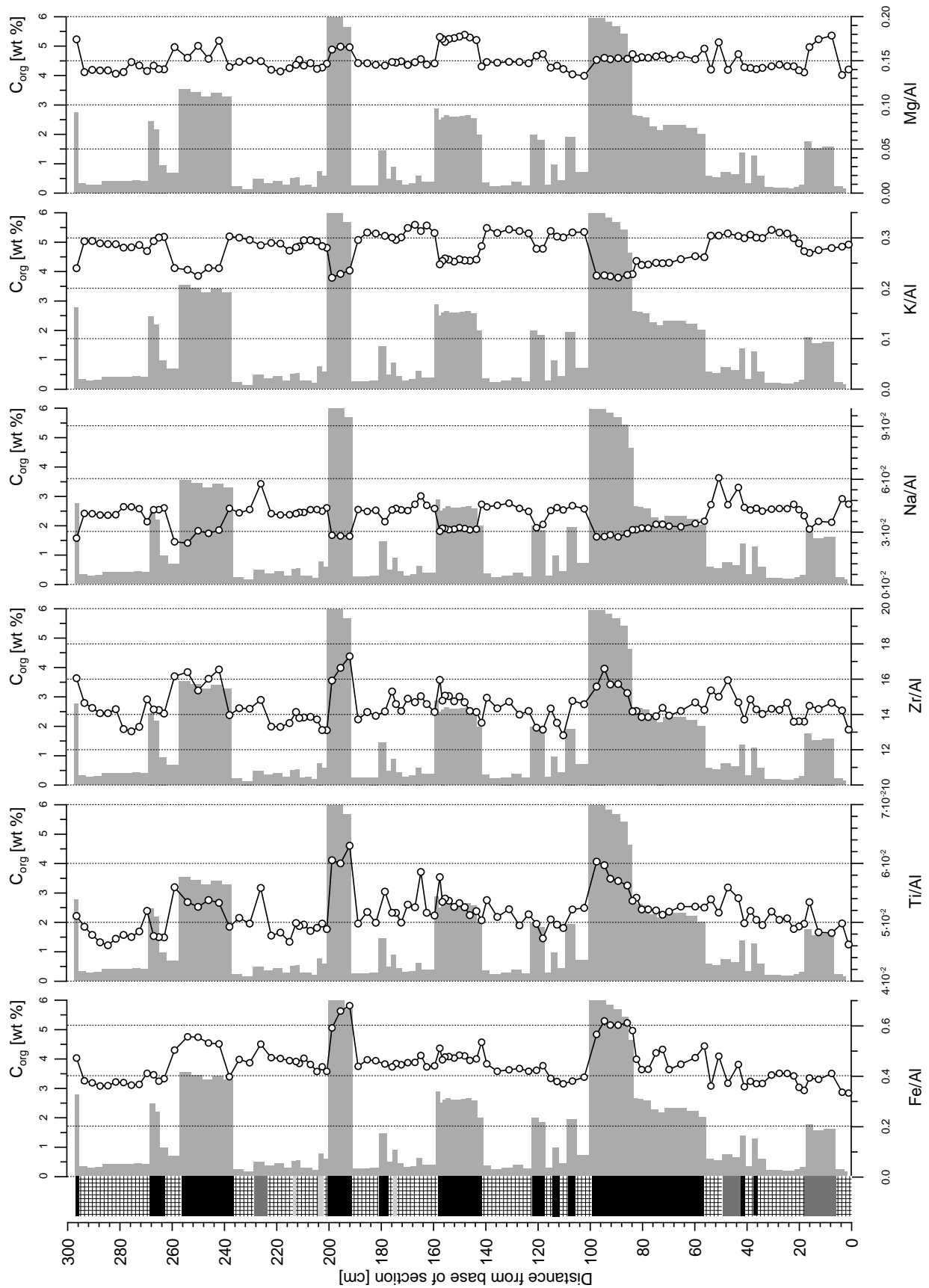


**Figure 4.** Elemental Fe/Al, Ti/Al, Zr/Al, Na/Al, K/Al, and Mg/Al ratios plotted against total organic carbon and lithology. Errors are only given if the size of the error bar would exceed the size of the symbol indicating the sampling point. For further explanations see caption of Figure 3.

**Table 1.** Compilation of the Random Errors of the Used Analytical Techniques.

Element	Unit	Detection Limit	Arithmetic Mean $\bar{x}$	Standard Deviation $s^2$	Absolute Error $\pm\Delta$	Relative Error % $\pm\delta$	Total Error After Normalizing With Al	
							Relative	Absolute
C <sub>Org</sub>	wt %	—	1.5	1.6	0.09	1.5	2.3	0.01
CaCO <sub>3</sub>	wt %	—	4	0.49	0.3	2.7	8.6	0.04
S	wt %	—	0.18	0.7	0.25	3.16	8.2	0.03
Si	wt %	0.02	29	2.74	0.09	0.3	1	0.03
Ti	wt %	0.01	0.44	0.03	0.003	0.74	0.8	0.0005
Al	wt %	0.03	8.2	0.04	0.066	0.8	—	—
Fe	wt %	0.01	3.7	0.55	0.13	3.5	4.5	0.015
Mn	wt %	8	1344	3468	32.58	2.9	7.4	4.05
Mg	wt %	0.01	1.25	0.1	0.01	1.15	1.65	0.001
Zr	ppm	2	120	8.3	1.17	1	1.8	0.28
Na	wt %	0.01	0.32	0.06	0.003	1	1.3	0.0004
K	wt %	0.01	2.3	0.2	0.03	1.4	1.5	0.003
P	wt %	0.0013	0.033	0.0055	0.0008	2.04	3.04	0.0001
Ba	ppm	40	380	48	10	2.7	4	1.6
Sr	ppm	2	115	15.35	1.1	0.94	1.4	0.17

All errors are given at a significance level of 95%. Arithmetic mean and standard deviation are calculated over all samples. Errors are calculated from repeated preparation and measurement of the same sample.

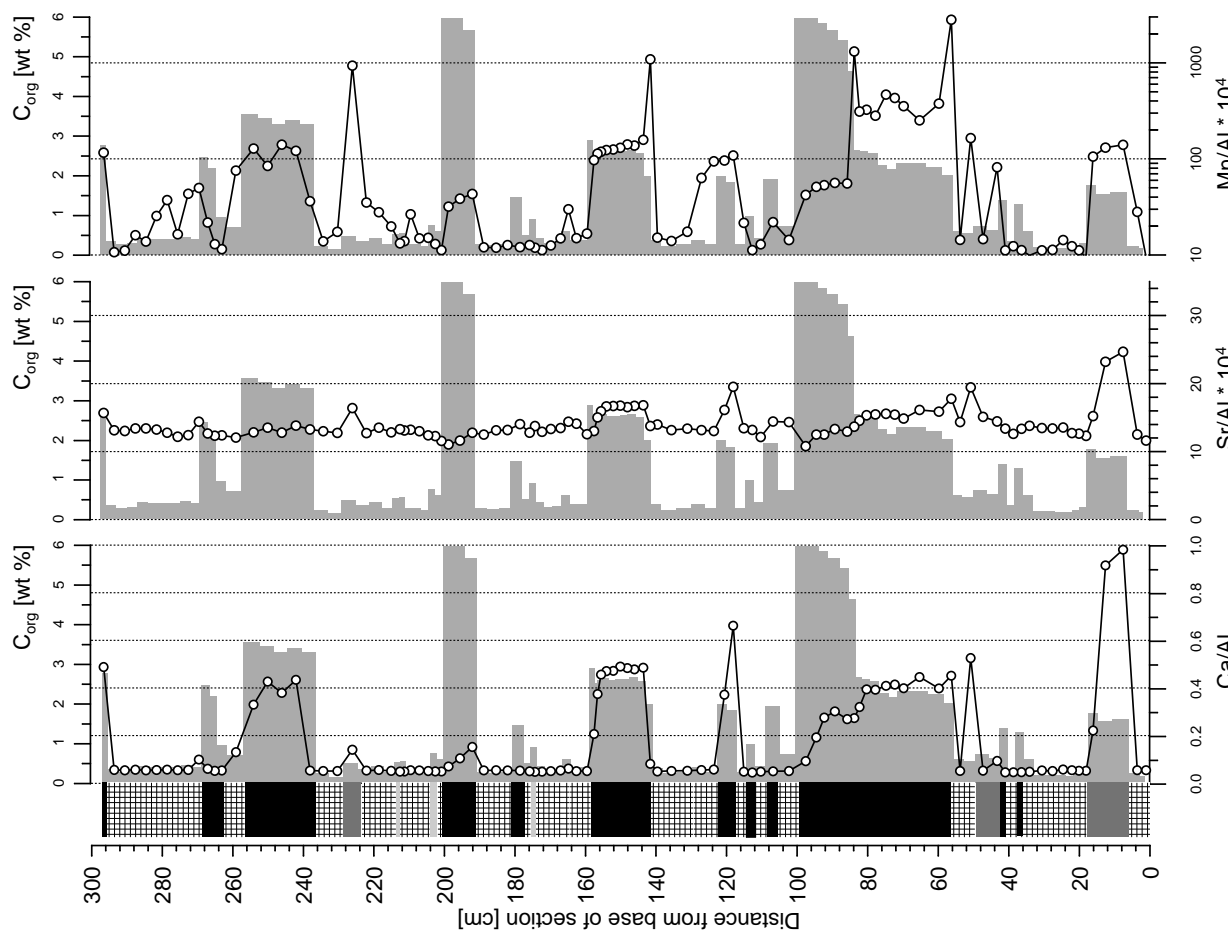


**Figure 5.** Elemental Ca/Al, Sr/Al and Mn/Al ratios plotted against TOC and lithology. For explanations see captions of Figs. 3 and 4.

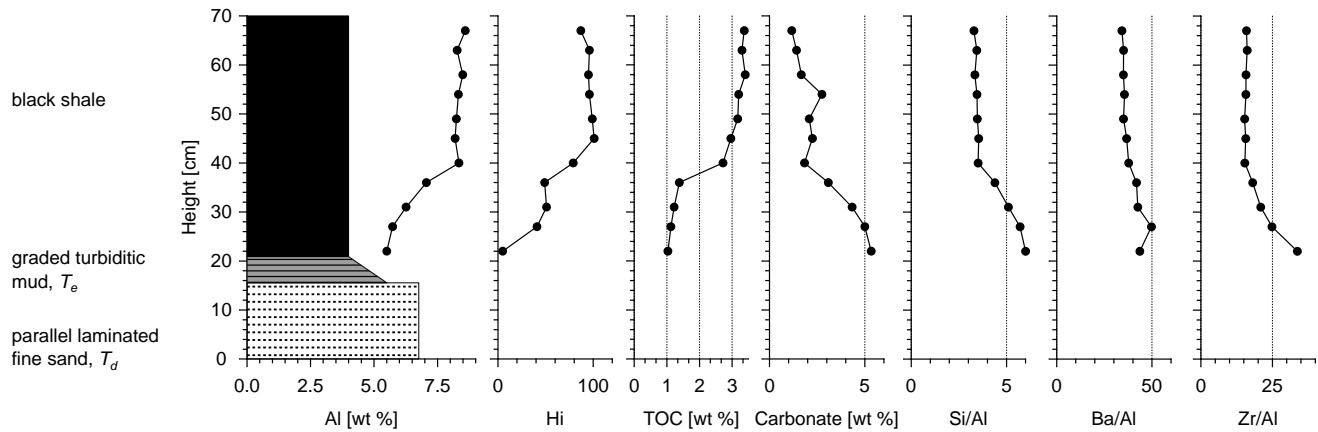


**Figure 8.** Chemical profiles above a thin turbidite outside the interval used for this study. The inorganic and organic composition of the lower 20 cm of the shale above the turbidite are different from the pelagic background sedimentation. Since turbidite-influenced shales possess such a clear geochemical signature, we can exclude turbidity current interference for the interval used for this study. We also calculated the HI following the method of *Langford and Blanc-Valleron* [1990], which yields an HI of 128. This suggests that (1) the HI decrease toward the turbidite might be caused by matrix effects (see also Figure 7) and (2) that HI values resulting from redeposition of organic matter are clearly different from the HI values of the background sedimentation. All ratios are given as weight percent ratios.

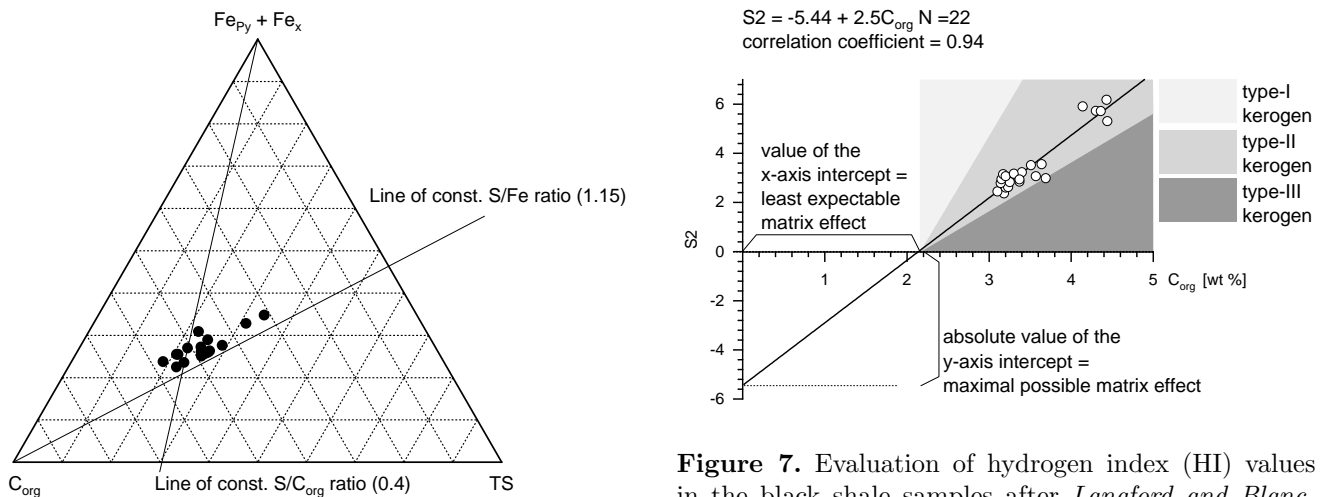


**Figure 6.** If samples plot along a line of constant S/C<sub>Org</sub> ratio, sulfate was a limiting factor in pyrite formation. If samples plot along a line of constant S/Fe ratio, pyrite formation was iron-limited. If no systematic relation is observable, sulfur limitation is likely [Dean and Arthur, 1989]. The S/Fe ratio of 1.15 has been chosen because it is the stoichiometric ratio of S and Fe in FeS<sub>2</sub>.

**Figure 7.** Evaluation of hydrogen index (HI) values in the black shale samples after *Langford and Blanc-Valleron* [1990]. HI is calculated from the slope of the regression line defined by the S<sub>2</sub> versus C<sub>Org</sub> as HI = 100 × slope = 250. The minimal matrix effect (i.e., HC adsorbed by the rock matrix and not contained in S<sub>2</sub>) corresponds to the value of the x axis intercept (= 2.2) in mg HC gr<sup>-1</sup> sample mass, and the maximal matrix effect to the absolute value of the y axis intercept (= 5.4) in mg HC gr<sup>-1</sup> sample mass.

endobenthic life and suggests anoxic conditions. Almost all elemental ratios show either an increase or decrease in elemental ratios when comparing a black with a green layer. It is tempting to attribute this coherent response to transport processes like redeposition of upslope material. However, no sedimentological indication of rede-

position (e.g., grain-size variations, bedding structures, etc.) has been found. To investigate the possibility of turbiditic interference, we analyzed a 50 cm long section above a thin (15 cm) turbidite. This section occurs 1 m above of the interval chosen for the present study. While the pelagic clays are characterized by almost constant Al values around 8.2 wt % with a standard deviation of

0.42, the clays above the turbidite show a significantly reduced Al content as low as 5.5 wt % (Figure 8). It is also apparent that the OM above the turbidite is significantly different from the OM raining down as pelagic background sedimentation. This demonstrates that although the top of the turbidite is indistinguishable from the pelagic background sedimentation by field methods, the turbidite still carries an ultrafine fraction that is able to deter the geochemical signal. However, this signal is geochemically well expressed. Thus we can reject the hypothesis that the investigated black/green shale cycles are caused by redeposition processes.

The Mn data of this study provide an unexpected picture: The green shales contain only minor amounts of Mn, while the black shales show values similar to the "average shale" [Wedepohl, 1971]. This suggests that the Mn content of black shales was controlled by the aluminosilicate fraction and implies that the black shales were deposited below an anoxic water column [Calvert and Pedersen, 1993].

The green shales constituted most likely a suboxic environment from which Mn was lost by "zone refining" [cf. Froehlich et al., 1979]. This notion is supported by the extremely high Mn values that can be observed at the base of some black shales layers and are interpreted as "frozen" Mn fronts. These fronts are most likely caused by a manganese-carbonate phase since Mn/Al shows a similar distribution as Ca/Al. This notion is in line with Calvert and Pedersen [1993] who noted that manganese carbonate can only be precipitated in places of active manganese pumping, i.e., when the redox boundary is at the sediment water interface. We therefore interpret these Mn fronts as the remains of a Mn pump, which depleted the underlying green shale and collapsed when the overlying water column changed from oxic to anoxic conditions.

Elemental ratios sensitive to changes in weathering conditions like Ti/Al, Zr/Al, and Mg/Al are enriched within the black shales; note that those increases are not caused by decreased Al values (see Figure 3). They can be either caused by intensification of weathering in the hinterland or by changing the source region. Since the timescales involved in the formation of a lateritic soil profile are in excess of  $10^6$  years, a changing source seems more likely. We thus assume that these variations are caused by changes in atmospheric circulation ("wind stress") or changes in the pathways of ocean currents. This interpretation is supported by the variation of the Na/Al and K/Al ratios, which are most likely caused by changes in clay mineral composition. The Fe/Al distribution mirrors mostly the variation of Zr/Al (e.g., the black shale at 190 cm in Figure 4). However, in some cases, significant differences can be observed (e.g., at 90 cm in Figure 4), and are interpreted as a result of early diagenetic diffusion of  $\text{Fe}^{2+}$  [Bernier, 1969].

Elemental ratios potentially sensitive to primary pro-

duction such as P/Al, Ba/Al, Si/Al, or  $\text{C}_{\text{Org}}/\text{Al}$ , are not equivocal. While P/Al and  $\text{C}_{\text{Org}}/\text{Al}$  are enriched in the black shales, Ba/Al and Si/Al are depleted. Both Si/Al and Ba/Al can be influenced by changes in the detrital composition. To exclude this possibility, we performed a statistical analysis to gain information about how many independent factors are needed to describe the observed elemental distribution.

To test the relationships between the analyzed elements, we employed the widely used technique of factor analysis [see, e.g., Heath and Dymond, 1981]. This type of statistical analysis tries to describe a larger set of variables by a smaller set of independent artificial variables. In the best case these synthetic variables can be attributed to real geological processes like dissolution, current transport, or hydrothermal input. However, assigning a synthetic factor to a specific process has to be done on grounds of geological reasoning.

The analysis was carried out using all 21 analyzed elements except Mn, but with the addition of the Ca/Sr ratio. Mn was excluded because of its non-Gaussian distribution. Factor analysis of a  $22 \times 22$  correlation matrix yields four synthetic variables (factors). Applying the "inverse correlation matrix test" yields a good diagonal matrix, which proves the suitability of the dataset for factor analysis [Backhaus et al., 1996]. The extraction of the principal factors by principal component analysis (PCA), was done using the "Quartimax" approach [Backhaus et al., 1996, see, e.g.,]. The results of the PCA were tested for stability by excluding different groups of elements and counter-checked by using a different extraction method ("Varimax") [Backhaus et al., 1996, see, e.g.,]. All tests yielded the same result; that is, the variation of most elements can be described by two major factors, accounting for ~60% of the observed variance, and two minor factors. If we group the element ratios according to their dominant factor, we get the following groups:

1. Ni/Al, Ti/Al, Co/Al, Fe/Al, P/Al, As/Al, Zr/Al,  $\text{C}_{\text{Org}}/\text{Al}$ , and S/Al. Most of these elements are clearly of detrital origin. Thus we conclude that the first factor describes the influence of detrital input.
2. Rb/Al, K/Al, Ba/Al, Sr/Ca, Na/Al, Ca/Al, Si/Al and Mg/Al. This factor combines elements that are sensitive to primary production and clay mineralogy.
3. The third factor (V/Al, Zn/Al, Cu/Al) is interpreted to represent diagenetic effects like redox mobilization.
4. Factor four, which has high loadings for Sr/Al, Th/Al, Mg/Al and Ca/Al, is probably associated with a phosphatic phase.

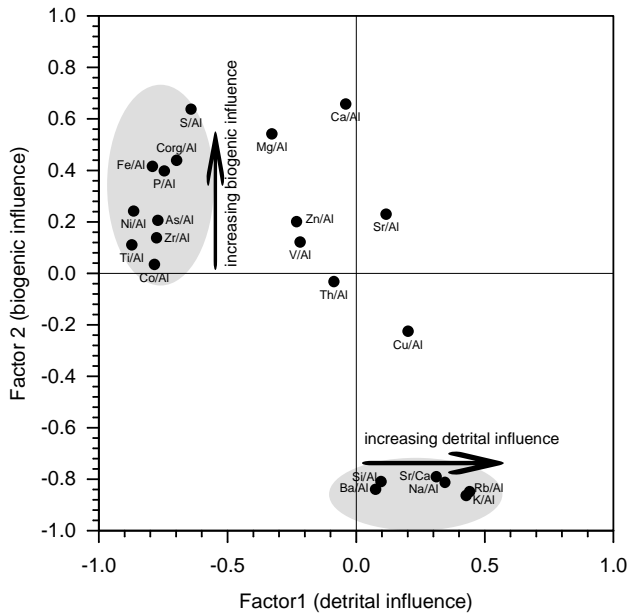


**Figure 9.** Distribution of elemental ratios when plotted within the detrital/biogenic coordinate system as yielded by principal component analysis.

While the interpretation of the two minor factors is somewhat speculative, the first two factors can clearly be interpreted to represent detrital and biogenic input, respectively.

Elements that are sensitive to detrital input as well as to biogenic sources (e.g.,  $C_{Org}/Al$  with its mixture of type II/III OM) should have high loadings for both factors. Figure 9 shows that this indeed is the case. Furthermore, most ratios group parallel to the factor axis, showing, for example, the increasing detrital influence when moving from  $Ba/Al$  to  $Rb/Al$  or from  $Co/Al$  to  $C_{Org}/Al$ . The clay-mineral associated elements like  $Rb$ ,  $Na$ , and  $K$  show high loadings for the detrital factor but also unexpectedly high loadings for factor 2 (biogenic input).

The factor analysis shows that  $Si/Al$  and  $Ba/Al$  have only minor loadings for the detrital factor, suggesting that the barium and silica signals are unlikely to be of detrital origin. However, barium is known to be mobile in reducing environments [see e.g., *Torres et al.*, 1996]. The main carrier phase of barium in seawater is suspended barite particles, which are collected by zooplankton and exported into the deeper waters via fast sinking fecal pellets [*Dehairs et al.*, 1980; *Dymond and Suess*, 1992; *Gingele and Dahmke*, 1994]. After incorporation into the sediment, biogenic barite can be mobilized below the sulfate reduction zone and diffuse upward until it reaches the base of the sulfate reduction zone where it reprecipitates as  $BaSO_4$  [*Torres et al.*, 1996]. In continental margin upwelling sites (e.g., Peru, Namibia, Oman), the sulfate reservoir is typically de-

pleted below 10–200 meters below the seafloor (mbsf) [see e.g., *Emeis and Morse*, 1993, Figure 5]. *Lasaga and Holland* [1976] have shown that a nonuniform distribution of OM in the sediment column does not necessarily result in a nonuniform composition of interstitial waters. They were able to show that to influence the composition of the interstitial waters, the frequency  $\alpha$  of the OM composition changes must be lower than

$$\alpha < \frac{\omega^2}{D_s}$$

where  $\omega$  stands for the sedimentation rate and  $D_s$  for the diffusion coefficient of sulfate. We assume that  $D_s = 5 \times 10^{-6}$  ( $cm^2 s^{-1}$ ) [*Krom and Berner*, 1980] and that our estimated sedimentation rate of  $9.4$   $mm kyr^{-1}$  has to be decompacted by a factor of 10. Thus we estimate a minimum value of 1.8 m.y. to cause deviations from the steady state behavior of the sulfate pore water profile. The same calculation for a sedimentation rate of  $26$   $mm kyr^{-1}$  (see below) yields a minimal time interval of 233 kyr. These times correspond to minimal sediment thicknesses (after compaction) of 17 and 6 m, respectively. In either case the black shale intercalations are too short to influence the sulfate distribution of the interstitial waters. That is, if barite dissolution has occurred, it occurred as a steady state process, affecting the green shales to the same degree as the black shales.

Because of this, we argue that the measured barite signal truly records changes in the pelagic background signal and was not affected by localized early diagenetic dissolution processes. This leaves us with the somewhat unexpected notion that the OM productivity was high during the green shale mode and low during the black shale mode.

The high DOP values, the well-preserved lamination of the black shales and the Mn distribution indicate that anoxic conditions occurred within the water column during the black shale deposition. Given that the anoxic conditions affected a sufficiently thick part of the water column, important consequences will result for the regeneration cycles of OM, barium, calcium, silica, and phosphorus. To investigate these consequences, we suggest the following very simple model.

For our model basin we assume an arbitrary water depth of 5000 meter below sea level (mbsl; see below for discussion). Following the data of *Betzer et al.* [1984], only 3.1% of the produced primary particulate organic matter (POM), normalized to an export production of  $100$   $g C m^{-2} yr^{-1}$  at 20 mbsl, reaches a depth of 5000 mbsl. Unfortunately, there are almost no data that compares primary productivity with the input of terrestrial organic matter (TOM). The data of *Westerhausen et al.* [1993] indicate however, that the contribution of TOM to the OM exported into the sediment is <18% if the offshore distance is >200 km. Because TOM is less easily oxidized [*Kolattukudy*, 1976; *Juniper and Jeffree*,

1983; *Gagosian and Peltzer*, 1986], the contribution of TOM to the exported OM must be even smaller. As a working hypothesis, we assume that 50% of the TOM input is exported at 5000 mbsl; thus the initial contribution of TOM compared to the primary production can be assumed to equal  $\sim 1\%$  of the primary production, which is in good agreement with existing data [*Gagosian and Peltzer*, 1986].

While most of the produced  $C_{Org}$  and carbonate is recycled in the water column, a small portion escapes destruction because it is incorporated into fast sinking particles [see e.g., *Grimm et al.*, 1997; *Honjo*, 1980]. After reaching the seafloor, these particles are either utilized by benthic organisms or subjected to oxidative breakdown, thus releasing the contained components. Because of the sub-CCD position of the sediment water interface, carbonate redissolves, but barium (as barite) and some silica (opal) get incorporated into the sediment (Figure 10).

Changing the system from green shale mode to black shale mode affects these regeneration cycles in several ways. With the establishment of anoxic conditions and a stratified water column the link of the photic zone to its most important nutrient supply, the phosphatic deepwater [*Ryan and Cita*, 1977], becomes weaker. Note that the suggested increase of P regeneration during anoxia [*Ingall et al.*, 1993; *Ingall and Jahnke*, 1994; *van Cappellen and Ingall*, 1994] is only effective for anoxic events occurring on timescales greater than the residence of P in the ocean ( $>50$  kyr) and is therefore not discussed in our model.

As a result of the weaker link, bioproduction and the export rate of  $C_{Org}$  decrease. It has been argued that OM degradation under anoxic conditions is of a similar magnitude as OM degradation under oxic conditions [e.g., *Kristensen and Blackburn*, 1987; *Canfield*, 1989b]. However, the degradation rate of refractory OM is much smaller under anoxic conditions, which leads to preferential preservation of degraded or refractory OM [*Canfield*, 1994]. Because the easily degradable OM has already been oxidized in the upper part of the water column, the influence of anoxia on OM preservation is depth dependent [*Canfield*, 1994]. We hypothesize that the bio-mediated breakdown of fecal pellets decreases under anoxic conditions too, which would provide a simple explanation for the occurrence of well-preserved coccoliths within the black shales. It is readily apparent that the almost exclusively fecal pellet controlled transport processes of barium [*Dehairs et al.*, 1980; *Dymond and Suess*, 1992; *Gingele and Dahmke*, 1994] are much less affected by changes of the oxygen content of the water column. The only way to introduce major changes to the regeneration cycle of barium is by barite dissolution in sulfate-depleted pore waters (see discussion above).

Assuming that barium content (and Si, which shows the same pattern as Ba) is linearly coupled to primary

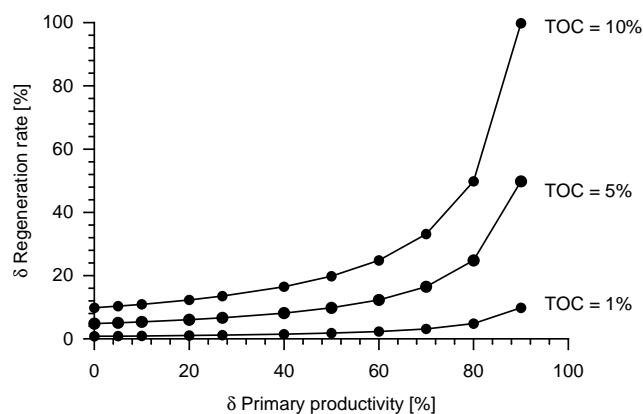


**Figure 11.** Assuming a linear relationship between primary production and OM exported into the sediment and fixing the model output to a constant TOC shows that large changes in primary production are easily compensated by small changes of the regeneration rate for a wide range of TOC values. The initial offset seen when the changes in primary productivity are zero shows the needed decrease in OM regeneration to change from normal TOC values (0.2%) to a given TOC level.

productivity and that the export of OM into the sediment is a linear function of primary production, we can calculate the consequences of this scenario. We assume that the input of TOM remains constant, that the breakdown of the TOM happens at the sediment/water interface, and that the average barium value of the green shales records 100 arbitrary productivity units (PU). Furthermore, we arbitrarily assume that these PUs correspond to 100 organic matter units (OMU) of which 99 units are marine and one unit is of detrital origin.

Within the black shales the barium-recorded  $C_{Org}$  productivity drops to an average of 73 PU. Thus the initial primary production (99 + 1) OMU drops to 72 + 1 = 73 OMU. As we know from the measured data, the buried amount of OM changes from 0.2% in the green shales to  $\sim 4.5\%$  in the black shales; thus the regenerated amount of OM equals 68.5 OMU. From this we can calculate the change in the regeneration rate of OM as from 99.8/100 = 99.8% to 68.44/73 = 93.7%, which is 6%. This calculation clearly shows that a slight (6%) decrease of the regeneration rate (including breakdown at the sediment water interface) overcompensates for the large (27%) decrease in primary productivity (Figure 10). Assuming a greater TOM regeneration rate amplifies this relationship even more. This calculation can be generalized and demonstrates that large changes in primary productivity require only small changes of the regeneration rate to maintain a constant TOC of the sediment (Figure 11).

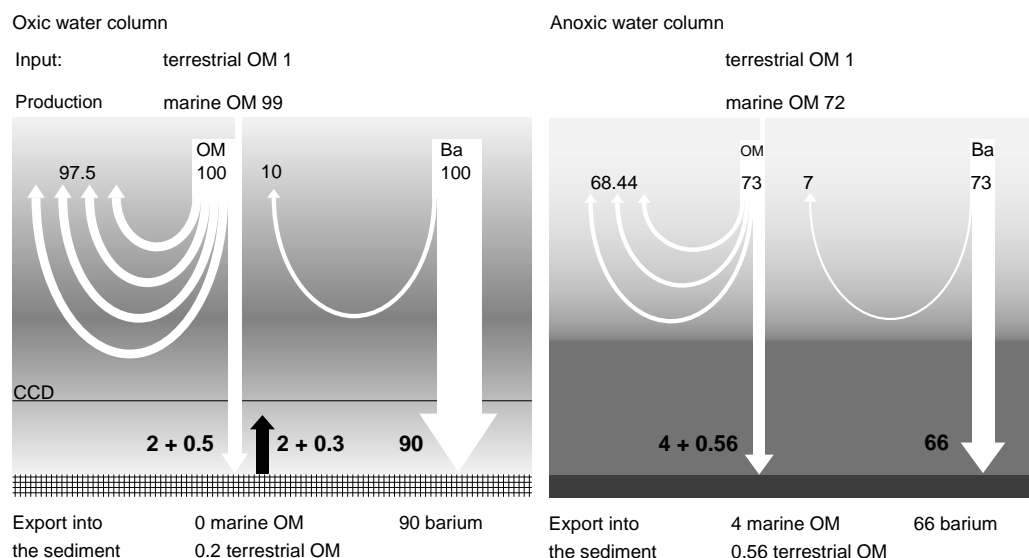


**Figure 10.** Simplified regeneration cycles of OM and barium during green and black shale deposition. The differences in the burial rates are a result of different transport mechanisms. While most  $C_{Org}$  is transported as particulate matter and already regenerated within the water column [Betzer *et al.*, 1984], barite is mainly transported in fast sinking fecal pellets [Dymond and Suess, 1992] and less affected by changes of the  $C_{Org}$  regeneration rate. The numbers represent hypothetical units but can be thought of as percentages.

## 2.2. Time Series Analysis

Time series analysis was carried out independently for all analyzed elements. Because of the very short interval of only 3 m, the data are noisy. Nevertheless, the spectral characteristics of the elements can be classified into several groups: (1) Elements that show only one peak around 52 cm wavelength, like Co/Al, Ti/Al and Zr/Al (e.g., Figure 12). This group comprises all detrital elements with a low loading for the biogenic factor (Figure 9). (2) Elements that show a clear bipartitioned peak around 52 cm wavelength, like Ba/Al (Figure 12). This group of elements consists of biogenically influenced elements with a low loading for the detrital factor. (3) Elements whose spectral power distribution can be explained as a superposition of the signal yielded for group 1 and group 2, respectively. That is, they are influenced by primary production as well as by detrital input, like  $C_{Org}/Al$  (Figure 12). (4) Elements that show no significant peaks at all (e.g., Mn/Al), which have been most likely subjected to diagenetic redistribution.

At the time when this study was designed, it was believed that the base of the section was Aptian in age [Hesse, 1973] and thus within the Cretaceous magnetic quiet zone. In consequence we selected the sampling site exclusively on the grounds of outcrop quality. However, recently generated  $\delta^{13}C_{Org}$  data (to be published elsewhere) show that the Rehbrengraben Formation extends at least to the middle Barremian. Geomag-

netic investigations currently in progress have successfully identified the magnetochron M1, and the preliminary data indicate the presence of the magnetochrons M3 and M0. We hope to have accurate time control for the black/green shale rhythms from the middle Barremian to the Early Aptian in the near future. If the refined data can be confirmed, the distance between the top of M3r and the base of M1r, which is 6 m, covers  $\sim 600$  kyr [Gradstein *et al.*, 1995]. The average black/green shale couplet thickness is 20 cm. Thus we obtain an average duration of 20 kyr per couplet and an average sedimentation rate of  $10 \text{ mm kyr}^{-1}$ ; suggesting that the black/green shale rhythms constitute a precessional signal.

## 3. Discussion

The data of the present study suggest that the investigated black shales are not the result of high primary production. Much of our reasoning is based on barium and silica, but we cannot categorically exclude the possibility that the observed barium and silica variations are diagenetic signals. Nevertheless, to our knowledge, there are no pore water profiles from modern marine upwelling sites where barium is mobilized within the first few centimeters bsf. As has been shown by Lasaga and Holland [1976], later sulfate depletion (and possible barium remobilization) must occur as a steady state process. The suggested model is valid over a large range of input parameters like the amount of contributed

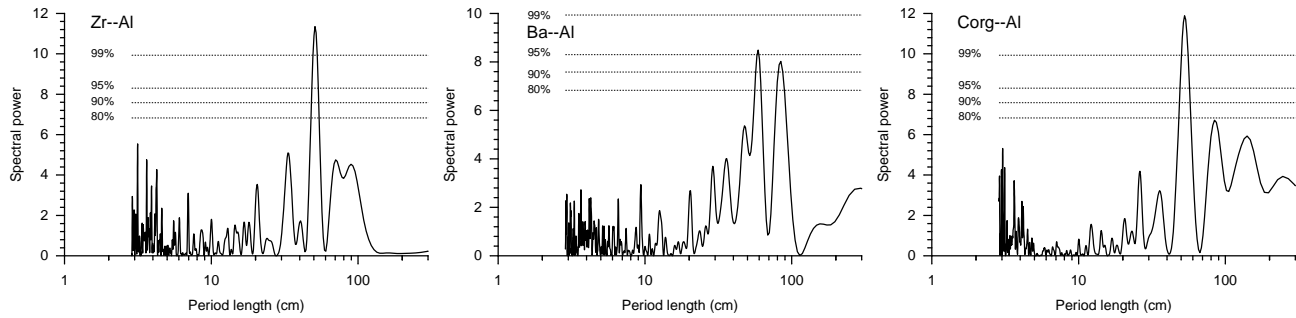


**Figure 12.** Powerspectra of various element ratios as obtained by the Lomb-Scargle Transform [Scargle, 1992]. The dotted horizontal lines indicate the significance level of the peak. Note the bipartitioning of the Ba/Al peak around 52 cm wave length and that the  $C_{Org}/Al$  peak (at 52 cm wavelength) is a superposition of the biogenic signal (i.e., Ba/Al) and the detrital signal (i.e., Zr/Al).

TOM or the assumed changes in primary productivity. Furthermore, if the investigated black shales were caused by enhanced production and enhanced preservation due to higher sedimentation rates [Canfield, 1989a; Calvert and Pedersen, 1992; Emeis and Morse, 1993], there are no data that support a fivefold increase of the sedimentation rate and the fivefold increase in primary productivity needed to explain the 25-fold increase of TOC. On the contrary, in many cases, the primary productivity during the Early Cretaceous was comparably low [Bralower and Thierstein, 1984; Premoli-Silva et al., 1989; Thierstein, 1989]. Besides the low-production/high-preservation origin of the cyclic black shales, the dataset displays a second interesting feature. Most black shale layers are associated with an increase of the detrital elements, which gives rise to the question of why the change of detrital composition covaries with the  $C_{Org}$  preservation.

### 3.1. A Depositional Model

As shown in the previous section, one way to interpret the elemental distribution patterns is by assuming that part of the water column has been anoxic during times of black shale deposition. However, what processes caused the anoxia? Examination of the paleogeographic position of the Early Cretaceous Tethys Ocean shows that it is situated between two distinct climate regimes (see Figure 13). The southern parts of the ocean were affected by the tropical low-pressure system (TL), while the northern parts were dominated by the subtropical high-pressure system (STH). The dry climate together with a trade wind system cause extremely high evaporation rates and, in turn, warm and saline surface waters. Computer simulation of salinity predicts values as high as 37‰ for places with high evaporation rates [Barron, 1995], sufficient to drive the generation of warm deep-water [Brass et al., 1981; Barron and Peterson, 1989].

However, such a system is sensitive to changes in the evaporation rate, which itself is a function of wind

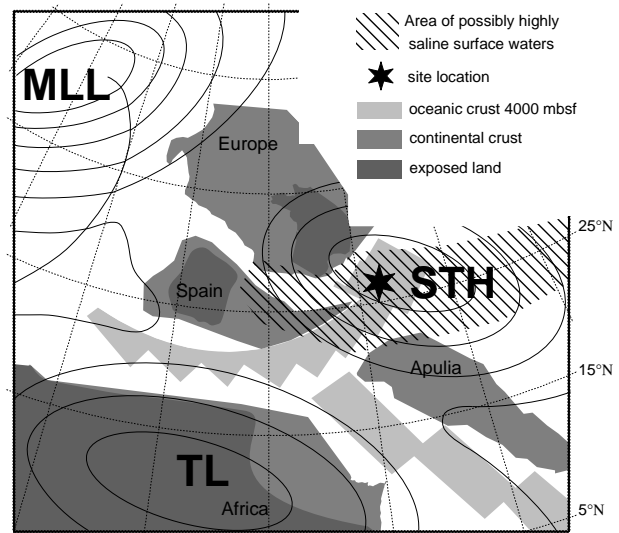


**Figure 13.** Principal elements of the Early Cretaceous climate in the Tethys region as depicted by most climate models [e.g., Oglesby and Park, 1989; Price et al., 1995; Barron, 1995; Hay et al., 1999a]: MLL, mid latitude-low pressure system; STH, subtropical high-pressure system, and TL, tropical low-pressure system. Coastlines are taken from Dercourt et al. [1993] but modified to suit the actual plate geometry. Depth of the ocean crust has been computed from ocean crust age as depth (meters) =  $2500 + 350 \times \sqrt{\text{age(m.y.)}}$ . Details on the plate-tectonic reconstruction will be published elsewhere.

speed, air humidity, insolation, and temperature [see, e.g., Barron et al., 1985]. Air humidity in particular will change as a function of the position of the intertropical convergence zone (ITCZ). In times of strongly developed midlatitude low-pressure systems (MLL), the ITCZ may short-circuit with the MLL, initiating a monsoonal event that transports humid air into the northern parts of the Tethys Ocean. The increased humidity decreases evaporation and increases precipitation and

possibly runoff from the bordering northern continents. Consequently, the salinity-driven deepwater generation is shut off and a stratified and oxygen-deficient water body may develop. This concept is supported by computer simulations investigating the effect of precession on climate. For example, the model run by *Oglesby and Park* [1989] for the middle Cretaceous showed that insolation changes exert a strong control on the monsoonal strength over proto-Asia and strongly influence evaporation/precipitation rates over the opening South Atlantic.

*Holser et al.* [1980] and *Hay and Wold* [1997] showed that the salinity of the lower Cretaceous ocean must have been higher than today. Changing the mean ocean salinity, as well as changing the salinity contrast within the ocean due to an increased hydrological cycle [*Hay*, 1995], changes the physical properties of water in many ways [*Rooth*, 1982]. Most notably, the temperature of maximum density is affected by salinity, which has sound consequences for the formation of deepwater [*Hay et al.*, 1999a]. *Schmidt and Mysak* [1996] were able to show that depending on salinity and temperature of the polar waters, the ocean can be in a metastable state, which neither favors polar nor tropical deepwater formation. It seems sensible to assume that such a metastable state is susceptible to external forcing. It should be noted that most of these climate simulations have been run to simulate a Cenomanian climate and that the Aptian boundary conditions were different. Most important, the South Atlantic was still closed (Figure 1). However, the Aptian/Albian is, similar to the Cenomanian, characterized by sediments with a well expressed cyclicity. Thus we propose that the concept of an “undecided ocean” (with respect to deepwater formation) susceptible to external forcing is a fruitful concept for the Early Cretaceous too.

### 3.2. Relation to Other Tethyan Black Shales

As stated in the introduction, most of the described Early Cretaceous black shales have been deposited on continental crust and thus in water depth >3000 mbsl and relatively near the continent. Our simple model indicates that the overall sedimentation rate, the position of the oxygen minimum zone, and the water depth play an important role in OM preservation (which is consistent with the findings of *Canfield* [1994]). Thus most of the currently known Tethyan black shales can probably not directly be compared with our scenario because they have been deposited in a shallower environment. However, they have been controlled by the same ocean/atmosphere interactions, and depending on the export-production/depth function, it might be conceivable to find black/green shale cycles in which black shales represent times of high organic production [see e.g., *Hofmann et al.*, 1999].

## 4. Conclusion

Geochemical analysis of Aptian sub-CCD black shales gives no indication for upwelling-induced high OM productivity. We can also exclude the possibility that the rhythmic black/green shale cycles are caused by reworking or massive input of detrital OM as suggested by *Habib* [1982]. Major-element distributions suggest that the analyzed black/green shale sequences record changes from a high-productivity and well-oxygenated green shale mode to a low-productivity and oxygen-deficient black shale mode. Furthermore, the data show that these changes covary with changes in the detrital composition. We therefore suggest that the anoxic periods are ultimately caused by climatic changes and that the link between climate and deep-sea sedimentation was a salinity-driven deepwater generation sensitive to changes of a possibly precession-influenced monsoonal system. This is analogous to a model proposed by *Baron et al.* [1985] for the Western Interior Seaway.

Furthermore, the results of the investigation show that the processes forming black shale layers in very deep marine basins (possibly significantly below the CCD) differ in many respects from the processes forming black shales in high-productivity upwelling areas at the shelf break. Most notably, the sedimentation rate is very low, and together with the great water depth, changes in the  $C_{Org}$  production rate cause only minor changes in the  $C_{Org}$  sedimentation rate whereas changes in  $C_{Org}$  preservation become the dominant control factor.

Time series analysis reveals that these changes are periodic in nature. However, because of a poorly constrained age model, we could not prove that the dominant periodicity in the investigated interval is indeed related to the precession component of the Milankovitch frequencies. Ongoing geomagnetic investigations will permit a reassessment of this problem in the near future.

**Acknowledgments.** We thank M. Wolf and W. Pickel (RWTH Aachen) for the optical characterization of the organic matter, as well as K.-H. Kirsch (LMU Univ. München), and K. von Salis Perch-Nielsen (ETH Zürich) for the identification of the coccoliths and dinoflagellates. H.-J. Brumsack (Oldenburg) provided supplemental XRF data to cross check our results. The comments of V. Rachold, P. Wignall, and H. Thierstein helped to improve an early version of this manuscript. T. Lyons, P. Meyers, and J. Park provided stimulating reviews, which we gratefully acknowledge. Finally, we would like to thank H. Weissert and N. Andersen for inspiring discussions, and J. McKenzie and J. Hauck for their support and encouragement. The project was funded by the “Deutsche Forschungsgemeinschaft” (German Science Foundation DFG) through their strategic grant program “Global and regional processes of biogenic sedimentation” under grant number Za-29/14.

## References

- Arthur, M. A., and I. Premoli Silva, Development of widespread organic carbon-rich strata in the mediterranean Tethys, in *Nature and Origin of Cretaceous Carbon-Rich Facies*, edited by S. O. Schlanger and M. B. Cita, pp. 7–54, Academic, San Diego, Calif., 1982.
- Backhaus, K., B. Erichson, W. Plinke, and R. Weiber, *Multivariate Analysemethoden*, 8 ed., Springer Verlag, New York, 1996.
- Barron, E. J., Tropical climate stability and implications for the distribution of life, in *Effects of Past Global Change on Life*, *Stud. Geophys.*, 14, pp. 108–117, Nat. Acad., Washington D.C., 1995.
- Barron, E. J., and W. H. Peterson, Model simulation of the Cretaceous ocean circulation, *Science*, 244, 684–686, 1989.
- Barron, E. J., M. A. Arthur, and E. G. Kauffman, Cretaceous rhythmic bedding sequences: A plausible link between orbital variations and climate, *Earth Planet. Sci. Lett.*, 72, 327–340, 1985.
- Berner, R. A., Migration of iron and sulfur within anaerobic sediments during early diagenesis, *Am. J. Sci.*, 267, 19–42, 1969.
- Berner, R. A., Sedimentary pyrite formation, *Am. J. Sci.*, 268, 1–23, 1970.
- Berner, R. A., Sulfate reduction and the rate of deposition of marine sediments, *Earth Planet. Sci. Lett.*, 37, 492–498, 1978.
- Betzer, P. R., W. J. Showers, E. A. Laws, C. D. Winn, G. R. DiTullio, and P. M. Kroopnick, Primary productivity and particle fluxes on a transect of the equator at 153°W in the Pacific Ocean, *Deep Sea Res., Part A*, 31, 1–11, 1984.
- de Boer, P. L., Cyclicity and storage of organic matter in middle Cretaceous pelagic sediments, in *Cyclic and Event Stratification*, edited by G. Einsele and A. Seilacher, pp. 456–474, Springer Verlag, New York, 1982.
- de Boer, P. L., and A. A. H. Wonders, Astronomically induced rhythmic bedding in Cretaceous pelagic sediments near Moria (Italy), in *Proceedings of the NATO Advanced Research Workshop on Milankovitch and Climate, Palisades, New York, U.S.A., November 30 – December 4, 1982*, edited by A. L. Berger, et al., *NATO ASI Series. Ser. C, Mathematical and Physical Sciences*, 126, pp. 177–190, Kluwer Academic Publishers, Dordrecht Holland, 1984.
- Bralower, T. J., and H. R. Thierstein, Low productivity and slow deep-water circulation in mid-Cretaceous oceans, *Geology*, 12, 614–618, 1984.
- Brass, G., E. Saltzman, J. Sloan, W. Hay, W. Holzer, and W. Peterson, Ocean circulation, plate tectonics and climate, in *Climate in Earth History*, *Stud. Geophys.*, 14, pp. 83–89, Nat. Acad., Washington D.C., 1981.
- Brumsack, H.-J., Geochemistry of Cretaceous black shales from the Atlantic Ocean (DSDP Legs 11, 14, 36 and 41), *Chem. Geol.*, 31, 1–25, 1980.
- Calvert, C. S., Simplified, complete CsCl-hydrazine-dimethylsulfoxide intercalation of kaolinite, *Clays Clay Miner.*, 32, 125–130, 1984.
- Calvert, S. E., and T. F. Pedersen, Organic carbon accumulation and preservation in marine sediments: How important is anoxia?, in *Organic Matter: Productivity, Accumulation, and Preservation in Recent and Ancient Sediments*, edited by J. K. Whelan and J. W. Farrington, pp. 231–263, Columbia University Press, New York, 1992.
- Calvert, S. E., and T. F. Pedersen, Geochemistry of recent oxic and anoxic marine sediments: Implications for the geological record, *Mar. Geol.*, 113, 67–88, 1993.
- Calvert, S. E., R. M. Bustin, and E. D. Ingall, Influence of water column anoxia and sediment supply on the burial and preservation of organic carbon in marine shales, *Geochim. Cosmochim. Acta*, 60, 1577–1593, 1996.
- Canfield, D. E., Reactive iron in marine sediments, *Geochim. Cosmochim. Acta*, 53, 619–632, 1989a.
- Canfield, D. E., Sulfate reduction and oxic respiration in marine sediments: Implications for the organic carbon preservation in euxinic environments, *Deep Sea Res., Part A*, 36, 121–138, 1989b.
- Canfield, D. E., Factors influencing organic carbon preservation in marine sediments, *Chem. Geol.*, 114, 315–329, 1994.
- van Cappellen, P., and E. D. Ingall, Benthic phosphorus regeneration, net primary production, and ocean anoxia: A model of the coupled marine biogeochemical cycles of carbon and phosphorus, *Paleoceanography*, 9, 677–692, 1994.
- Chamley, H., and C. Robert, Paleoenvironmental significance of clay deposits in Atlantic black shales, in *Nature and Origin of Cretaceous Carbon-rich Facies*, edited by S. O. Schlanger and M. B. Cita, pp. 101–112, Academic, San Diego, Calif., 1982.
- Dean, W. E., and M. A. Arthur, Iron-sulfur-carbon relationships in organic-carbon-rich sequences I: Cretaceous Western Interior Seaway, *Am. J. Sci.*, 289, 708–743, 1989.
- Dean, W. E., and J. V. Gardner, Origin and geochemistry of redox cycles of Jurassic to Eocene age, Cape Verde Basin (DSDP Site 367), continental margin of northwest Africa, in *Nature and Origin of Cretaceous Carbon-rich Facies*, edited by S. O. Schlanger and M. B. Cita, pp. 55–78, Academic, San Diego, Calif., 1982.
- Dean, W. E., J. V. Gardner, L. F. Jansa, P. Čepek, and E. Seibold, Cyclic sedimentation along the continental margin of Northwest Africa, *Initial Rep. Deep Sea Drill. Proj.*, 41, 965–986, 1978.
- Degens, E. T., and P. Stoffers, Stratified waters as a key to the past, *Nature*, 263, 22–27, 1976.
- Dehairs, F., R. Chesselet, and J. Jedwab, Discrete suspended particles of barite and the barium cycle in the open ocean, *Earth Planet. Sci. Lett.*, 49, 528–550, 1980.
- Dercourt, J., L. E. Ricou, and B. Vrielynck (Eds.), *Atlas Tethys Palaeoenvironmental Maps*, Gauthier-Villars, Paris, 1993.
- Dymond, J., and E. Suess, Barium in deep-sea sediment: A geochemical proxy for paleoproductivity, *Paleoceanography*, 7, 163–181, 1992.
- Emeis, K. C., and J. W. Morse, Zur Systematik der Kohlenstoff-Schwefel-Eisen-Verhältnisse in Auftriebs sedimenten, *Geol. Rundsch.*, 82, 604–618, 1993.
- Espitalié, J., G. Deroo, and F. Marquis, La pyrolyse Rock-Eval et ses applications, *Rev. Inst. Fr. Pet.*, 40, 563–579, 1985a.
- Espitalié, J., G. Deroo, and F. Marquis, La pyrolyse Rock-Eval et ses applications, *Rev. Inst. Fr. Pet.*, 40, 755–784, 1985b.
- Fischer, A. G., T. D. Herbert, G. Napoleone, I. Premoli Silva, and M. Ripepe, Albian pelagic rhythms (Piobbico Core), *J. Sediment. Petrol.*, 61, 1173–1193, 1991.

- Froehlich, P. N., et al., Early oxidation of organic matter in pelagic sediments of the eastern equatorial Atlantic: Suboxic diagenesis, *Geochim. Cosmochim. Acta*, *43*, 1075–1090, 1979.
- Gagosian, R. B., and E. T. Peltzer, The importance of atmospheric input of terrestrial organic material to deep-sea sediments, *Org. Geochem.*, *10*, 661–669, 1986.
- Gingele, F., and A. Dahmke, Discrete barite particles and barium as tracers of paleoproductivity in South Atlantic sediments, *Paleoceanography*, *9*, 151–168, 1994.
- Gradstein, F. M., F. P. Agterberg, J. G. Ogg, J. Hardenbol, P. van Veen, J. Thierry, and Z. Huang, A Triassic, Jurassic and Cretaceous time scale, in *Geochronology, Time Scales and Global Stratigraphic Correlation*, edited by W. A. Berggren, et al., *Spec. Publ. SEPM Soc. Sediment. Geol.*, *54*, pp. 95–126, 1995.
- Grimm, K. A., C. B. Lange, and A. S. Gill, Self-sedimentation of phytoplankton blooms in the geologic record, *J. Sediment. Petrol.*, *110*, 151–161, 1997.
- Habib, D., Sedimentary supply origin of Cretaceous black shales, in *Nature and Origin of Cretaceous Carbon-rich Facies*, edited by S. O. Schlanger and M. B. Cita, pp. 113–127, Academic, San Diego, Calif., 1982.
- Hauck, J., Paläomagnetische Untersuchungen an ausgewählten Profilen der Kreide in der Rhenodanubischen Flysch-Zone, Ph.D. thesis, Inst. Geophys. Ludwig-Maximilians-Univ. Munich, Germany, 1998.
- Hay, W. W., Cretaceous Paleogeography, *Geol. Carpathica*, *46*, 257–266, 1995.
- Hay, W. W., and C. N. Wold, Preliminary reconstruction of the salinity of the ocean in the Cenozoic and Mesozoic, in *C468 Geowissenschaften-Paläontologie, Stratigraphie, Fazies, Freiburger Forsch.*, *5*, 1997, Karl-Armin-Tröger-Festschrift.
- Hay, W. W., S. Voigt, R. M. DeConto, and C. N. Wold, Paleoclimate and Circulation of Cretaceous Oceans, in *Biogenic sedimentation: Results of the DFG special interest programme. Lecture Notes in Earth Sciences*, Springer Verlag, New York, 1999a.
- Hay, W. W., et al., An alternative global Cretaceous paleogeography, in *The Evolution of Cretaceous Ocean/Climate Systems*, edited by E. Barrera and C. Johnson, *Geol. Soc. Am. Spec. Publ.*, *332*, pp. 1–47, 1999b, <http://www.odsn.de/odsn/services/paleomap/paleomap.html>.
- Heath, R. G., and J. Dymond, Metalliferous-sediment deposition in time and space: East Pacific Rise and Bauer Basin, northern Nazca Plate, in *Nazca Plate: Crustal Formation and Andean Convergence*, edited by L. D. Kulm, et al., *Geol. Soc. Am. Mem.*, *154*, pp. 175–197, 1981.
- Hesse, R., Flysch-Gault und Falknis-Tasna-Gault (Unterkreide): Kontinuierlicher Übergang von der distalen zur proximalen Flyschfazies auf einer penninischen Trogebene der Alpen, *Geol. Palaeontol.*, *SB 2*, 1–90, 1973.
- Hesse, R., Long-distance continuity of turbidites: Possible evidence for an Early Cretaceous trench–abyssal plain in the East Alps, *Geol. Soc. Am. Bull.*, *85*, 859–870, 1974.
- Hesse, R., Turbiditic and non-turbiditic mudstone of Cretaceous flysch sections of the East Alps and other basins, *Sedimentology*, *22*, 387–416, 1975.
- Hesse, R., Cretaceous–Palaeogene Flysch Zone of the East Alps and Carpathians: identification and plate-tectonic significance of ‘dormant’ and ‘active’ deep-sea trenches in the Alpine-Carpathian Arc, in *Trench-Forearc Geology*, edited by J. K. Leggett, *Geol. Soc. Spec. Publ.*, *10*, pp. 471–494, 1982.
- Hesse, R., and A. Butt, Paleobathymetry of Cretaceous turbidite basins of the East Alps relative to the calcite compensation level, *J. Geol.*, *84*, 505–533, 1976.
- Hofmann, P., W. Ricken, L. Schwark, and D. Leythaeuser, Coupled oceanic effects of climatic cycles from late Albian deep-sea sections of the North Atlantic, in *The evolution of the Cretaceous ocean/climate systems*, edited by E. Barrera and C. Johnson, *Geol. Soc. Am. Spec. Publ.*, 1999.
- Holser, W. T., W. W. Hay, D. E. Jory, and W. J. O’Connell, A census of evaporites and its implications for oceanic geochemistry, in *Geol. Soc. Am. Abstr. Programs*, *20*, 448, 1980.
- Honjo, S., Material fluxes and modes of sedimentation in the mesopelagic and bathypelagic zones, *J. Mar. Res.*, *38*, 53–97, 1980.
- Hsü, J. K., Alpine flysch in a Mediterranean setting, *Proc. Int. Geol. Congr.*, *6*, 67–74, 1972.
- Ingall, E. D., and R. Jahnke, Evidence for enhanced phosphorus regeneration from marine sediments overlain by oxygen depleted waters, *Geochim. Cosmochim. Acta*, *58*, 2571–2575, 1994.
- Ingall, E. D., R. M. Bustin, and P. V. Capellen, Influence of water column anoxia on the burial and preservation of carbon and phosphorus in marine shales, *Geochim. Cosmochim. Acta*, *57*, 303–316, 1993.
- Jansa, L. F., P. Enos, B. E. Tucholke, F. M. Gradstein, and R. E. Sheridan, Mesozoic–Cenozoic sedimentary formations of the North Atlantic basin; western North Atlantic, in *Deep Drilling Results in the Atlantic Ocean: Continental Margins and Paleoenvironment*, edited by M. Talwani, W. W. Hay, and W. B. F. Ryan, *Maurice Ewing Ser.*, *3*, pp. 1–57, AGU, Washington, D.C., 1979.
- Juniper, B. E., and C. E. Jeffree, *Plant Surfaces*, Edward Arnold, London, 1983.
- Keil, R. G., D. B. Montluçon, F. G. Prahl, and J. I. Hedges, Sorptive preservation of labile organic matter in marine sediments, *Nature*, *370*, 549–552, 1994.
- Kolattukudy, P. E., *Chemistry and Biochemistry of Natural Waxes*, Elsevier, New York, 1976.
- Kristensen, E., and T. H. Blackburn, The fate of organic carbon and nitrogen in experimental marine sediment systems: Influence of bioturbation and anoxia, *J. Mar. Res.*, *45*, 231–257, 1987.
- Krom, M. D., and R. A. Berner, The diffusion coefficients of sulfate, ammonium, and phosphate ions in anoxic marine sediments, *Limnol. Oceanogr.*, *25*, 327–337, 1980.
- Langford, F. F., and M. M. Blanc-Valleron, Interpreting Rock-Eval pyrolysis data using graphs of pyrolyzable hydrocarbons vs. total organic carbon, *AAPG Bull.*, *74*, 799–804, 1990.
- Lasaga, A. C., and H. D. Holland, Mathematical aspects of non-steady-state diagenesis, *Geochim. Cosmochim. Acta*, *40*, 257–266, 1976.
- Leventhal, L., and C. Taylor, Comparison of methods to determine degree of pyritization, *Geochim. Cosmochim. Acta*, *54*, 2621–2625, 1990.
- McCave, I. N., Depositional features of organic carbon-rich black and green mudstones at DSDP sites 386 and 387, western North Atlantic, *Initial Rep. Deep Sea Drill. Proj.*, *43*, 411–416, 1979.

- Murray, R. W., M. Leinen, and A. R. Isern, Biogenic flux of Al to the sediment in the central equatorial Pacific Ocean: Evidence for increased productivity during glacial periods, *Paleoceanography*, 8, 651–670, 1993.
- Oglesby, R., and J. Park, The effect of precessional insolation changes on the Cretaceous climate and cyclic sedimentation, *J. Geophys. Res.*, 94, 17,793–14,816, 1989.
- Park, J., and T. D. Herbert, Hunting for paleoclimatic periodicities in a geologic time series with an uncertain time scale, *J. Geophys. Res.*, 92, 14,027–14,040, 1987.
- Pedersen, T. F., and S. E. Calvert, Anoxia vs. productivity: what controls the formation of organic-carbon-rich sediments and sedimentary rocks, *AAPG Bull.*, 74, 454–466, 1990.
- Premoli-Silva, I., E. Erba, and M. E. Tornaghi, Paleoenvironmental signals and changes in surface fertility in mid Cretaceous C<sub>org</sub>-rich pelagic facies of the Fucoïd Marls (Central Italy), *Geob. mem. spec.*, 11, 225–236, 1989.
- Price, G. D., B. W. Sellwood, and P. J. Valdes, Sedimentological evaluation of general circulation model simulations for the “greenhouse” Earth: Cretaceous and Jurassic case studies., *Sediment. Geol.*, 100, 159–180, 1995.
- Raiswell, R., and R. A. Berner, Pyrite formation in euxinic and semi-euxinic sediments, *Am. J. Sci.*, 285, 710–724, 1985.
- Raiswell, R., and R. A. Berner, Pyrite and organic matter in Phanerozoic normal marine shales, *Geochim. Cosmochim. Acta*, 50, 1967–1976, 1986.
- Raiswell, R., F. Buckley, R. A. Berner, and T. F. Anderson, Degree of pyritization of iron as a paleoenvironmental indicator of bottom-water oxygenation, *J. Sediment. Petrol.*, 58, 812–819, 1988.
- Rooth, P. H., Mesozoic paleoceanography of the North Atlantic and Tethys Oceans, in *North Atlantic Paleoceanography*, edited by C. P. Summerhayes and N. J. Shackleton, *Geol. Soc. Spec. Publ.*, 21, pp. 299–320, 1982.
- Ryan, W. B. F., and M. B. Cita, Ignorance concerning episodes of ocean-wide stagnation, *Mar. Geol.*, 23, 197–215, 1977.
- Scargle, J. D., Deconvolution of chaotic and random time series, in *Statistics in the Environmental and Earth Sciences*, edited by A. T. Walden and P. Guttorp, pp. 119–136, Halsted, New York, 1992.
- Schlanger, S. O., and H. C. Jenkyns, Cretaceous oceanic anoxic events: causes and consequences, *Geol. Mijnbouw*, 55, 179–184, 1976.
- Schmidt, G. A., and L. A. Mysak, Can increased poleward oceanic heat flux explain the warm Cretaceous climate?, *Paleoceanography*, 11, 579–593, 1996.
- Sissingh, W., Microfossil biostratigraphy and stage-stratotypes of the Cretaceous, *Geol. Mijnbouw*, 57, 433–440, 1978.
- Teichmüller, M., and B. Durand, Fluorescence microscopical rank studies on liptinites and vitrinites in peat and coals, and comparison with results of the rock-eval pyrolysis, *Int. J. Coal Geol.*, 2, 197–230, 1983.
- Thierstein, H. R., Inventory of paleoproductivity records: the Mid-Cretaceous Enigma, in *Productivity of the Ocean: Present and Past*, edited by W. H. Berger, V. S. Smetacek, and G. Wefer, pp. 355–375, John Wiley, New York, 1989.
- Tissot, B. P., and D. H. Welte, *Petroleum Formation and Occurrence*, 2 ed., Springer Verlag, New York, 1984.
- Torres, M. E., H.-J. Brumsack, G. Bohrmann, and K. C. Emeis, Barite fronts in continental margin sediments: A new look at barium remobilization in the zone of sulfate reduction and formation of heavy barites in diagenetic fronts, *Chem. Geol.*, 127, 125–139, 1996.
- Tyson, R. V., The genesis and palynofacies characteristics of marine petroleum source rocks, in *Marine petroleum source rocks*, edited by J. Brooks and A. J. Fleet, *Geol. Soc. Spec. Publ.*, 26, pp. 47–67, Geol. Soc., 1987.
- Vetters, H., Geologische Karte der Republik Österreich, 1:500 000, *Geol. Bundesanst., Austria*, 1923, 3rd. unchanged reprint 1980.
- Wedepohl, K. H., Environmental influence on the chemical composition of shales and clays, in *Physics and Chemistry of the Earth*, edited by L. H. Ahrens, et al., 8, 1 ed., pp. 307–333, Pergamon, Tarrytown, New York, 1971.
- Weissert, H., J. McKenzie, and P. Hochuli, Cyclic anoxic events in the Early Cretaceous Tethys Ocean, *Geology*, 7, 147–151, 1978.
- Westerhausen, L., J. Poynter, G. Eglinton, H. Erlenkeuser, and M. Sarnthein, Marine and terrigenous origin of organic matter in modern sediments of the equatorial east Atlantic: The  $\delta^{13}\text{C}_{\text{Org}}$  and molecular record, *Deep Sea Res.*, 40/I, 1087–1121, 1993.
- Wortmann, U. G., Zur Ursache der hemipelagischen schwarz/grün Zyklen im Apt/Alb der bayerischen Flyschzone, Ph.D. thesis, Lehrstuhl für Allg., Ang. und Ing. Geol., TU-München, Germany, 1996, <http://www.spoc.ethz.ch/uli/papers/diss/index.html>.
- Wortmann, U. G., Early Cretaceous Tethys major-element data, IGBP PAGES/World Data Cent.-A for Paleoclimatol. Data Contrib. Ser. #1999-009, Natl. Oceano. and Atmos. Admin./Natl. Geophys. Data Cent. Paleoclimatol. Program, Boulder, Colo., 1999, [http://www.ngdc.noaa.gov:8800/paleo/plsql/cs\\_search](http://www.ngdc.noaa.gov:8800/paleo/plsql/cs_search).
- R. Hesse, Department of Earth and Planetary Sciences, McGill University, 3450 University St., Montréal, Québec, H3A 2A7 Canada.
- U. G. Wortmann, Geological Institute, Eidgenössische Technische Hochschule, Zürich, Sonneggstr. 5, CH-8092 Zürich, Switzerland, [www.spoc.ethz.ch](http://www.spoc.ethz.ch)
- W. Zacher, Lehrstuhl für Allgemeine, Angewandte und Ingenieur-Geologie der Technischen Universität München, Lichtenbergstr. 4, D – 85748 Garching, Germany  
email: [hesserzn@mailhost.rz.ruhr-uni-bochum.de](mailto:hesserzn@mailhost.rz.ruhr-uni-bochum.de), [uliw@erdw.ethz.ch](mailto:uliw@erdw.ethz.ch)

Received May 18, 1998; revised February 26, 1999; accepted March 10, 1999.

This preprint was prepared with AGU's L<sup>A</sup>T<sub>E</sub>X macros v5.01, with the extension package ‘AGU++’ by P. W. Daly